

## Generation of electron beams from a laser wakefield acceleration in pure neon gas

Song Li, Nasr A. M. Hafz, Mohammad Mirzaie, Ahmed M. M. Elsied, Xulei Ge, Feng Liu, Thomas Sokollik, Mengze Tao, Liming Chen, Min Chen, Zhengming Sheng, and Jie Zhang

Citation: *Physics of Plasmas* (1994-present) **21**, 083108 (2014); doi: 10.1063/1.4892557

View online: <http://dx.doi.org/10.1063/1.4892557>

View Table of Contents: <http://scitation.aip.org/content/aip/journal/pop/21/8?ver=pdfcov>

Published by the [AIP Publishing](#)

---

### Articles you may be interested in

[High-quality electron beam from laser wake-field acceleration in laser produced plasma plumes](#)

*Appl. Phys. Lett.* **102**, 231108 (2013); 10.1063/1.4810012

[Generation of tunable, 100–800 MeV quasi-monoenergetic electron beams from a laser-wakefield accelerator in the blowout regime](#)

*Phys. Plasmas* **19**, 056703 (2012); 10.1063/1.4718711

[Self-mode-transition from laser wakefield accelerator to plasma wakefield accelerator of laser-driven plasma-based electron acceleration](#)

*Phys. Plasmas* **17**, 123104 (2010); 10.1063/1.3522757


[Ultrashort high quality electron beam from laser wakefield accelerator using two-step plasma density profile](#)


*Rev. Sci. Instrum.* **81**, 033307 (2010); 10.1063/1.3360927

[GeV electron beams from a centimeter-scale channel guided laser wakefield accelerator](#)


*Phys. Plasmas* **14**, 056708 (2007); 10.1063/1.2718524

---

A collection of Pfeiffer Vacuum industrial equipment, including a red turbopump, a silver turbopump, a silver backing pump, a red turbopump with a long shaft, and a silver chamber component.

 Vacuum Solutions from a Single Source

- Turbopumps
- Backing pumps
- Leak detectors
- Measurement and analysis equipment
- Chambers and components

**PFEIFFER**  **VACUUM**

## Generation of electron beams from a laser wakefield acceleration in pure neon gas

Song Li,<sup>1</sup> Nasr A. M. Hafz,<sup>1,a)</sup> Mohammad Mirzaie,<sup>1</sup> Ahmed M. M. Elsied,<sup>1</sup> Xulei Ge,<sup>1</sup> Feng Liu,<sup>1</sup> Thomas Sokollik,<sup>1</sup> Mengze Tao,<sup>2</sup> Liming Chen,<sup>2</sup> Min Chen,<sup>1</sup> Zhengming Sheng,<sup>1</sup> and Jie Zhang<sup>1,b)</sup>

<sup>1</sup>Key Laboratory for Laser Plasmas (MOE) and Department of Physics and Astronomy, Shanghai Jiao Tong University, Shanghai 200240, China

<sup>2</sup>Beijing National Laboratory of Condensed Matter Physics, Institute of Physics, Chinese Academy of Sciences, Beijing 100190, China

(Received 1 February 2014; accepted 28 July 2014; published online 7 August 2014)

We report on the generation of quasimonoenergetic electron beams by the laser wakefield acceleration of 17–50 TW, 30 fs laser pulses in pure neon gas jet. The generated beams have energies in the range 40–120 MeV and up to  $\sim 430$  pC of charge. At a relatively high density, we observed multiple electron beamlets which has been interpreted by simulations to be the result of breakup of the laser pulse into multiple filaments in the plasma. Each filament drives its own wakefield and generates its own electron beamlet. © 2014 AIP Publishing LLC.

[<http://dx.doi.org/10.1063/1.4892557>]

Since the concept of laser wakefield acceleration (LWFA) was proposed by Tajima and Dawson<sup>1</sup> in 1979, many laboratories around the world have done extensive and in-depth studies in this field. This scheme utilizes relativistic large amplitude plasma waves driven by laser pulses of relativistic intensities for accelerating electrons to relativistic energies within extremely short distances, realizing extremely high accelerating gradients (exceeding 100 GeV/m).<sup>2–5</sup> So it is a scheme for building table-top accelerators based on ultra-intense table-top lasers. Electron beams with energy near and over 1 GeV have been experimentally demonstrated by using gas jets,<sup>2,3,6,7</sup> gas cells,<sup>4,6</sup> and capillary discharge waveguides.<sup>5</sup> In traditional self-injection LWFA, pure helium<sup>2,3,6–8</sup> or hydrogen<sup>5</sup> gases (plasmas) are generally used as the interaction media to accelerate the electrons. However, the electron energy was limited by the dephasing length to the range of 0.7–1 GeV using gas-jet targets, even very high laser powers or high densities were used to initiate the self-injection.<sup>2,3,6,7</sup> Leemans *et al.*<sup>5</sup> used a hydrogen capillary discharge waveguide with lower density to obtain longer interaction lengths over which acceleration occurred to gain high-quality electron bunches with the energy up to 1 GeV.

Recently, ionization-induced injection mechanism has been proposed and demonstrated to have some advantages over the self-injection, such as generating energetic electrons under lower laser intensity thresholds,<sup>9</sup> increasing the beam charge and lowering the beam divergence.<sup>10,11</sup> Using this mechanism, Clayton *et al.*<sup>4</sup> used a 1.3 cm long gas cell by mixing controlled amounts of CO<sub>2</sub> in He with the plasma density below  $1.5 \times 10^{18} \text{ cm}^{-3}$  to generate a continuous electron beam with a maximum energy up to 1.45 GeV. Mo *et al.*<sup>12</sup> also reported 500 MeV–1 GeV quasimonoenergetic electron bunches using ionization injection in mixtures of 4%–10% of CO<sub>2</sub> in He.

Applications such as the x-ray generation through Compton scattering<sup>13</sup> or betatron oscillation<sup>14</sup> require electron beams with ever high charge and small divergence, which can be generated by using higher Z gases. A few experiments<sup>15–18</sup> have reported quasimonoenergetic electron beams with the energy of 7–50 MeV using pure nitrogen gas jet plasmas driven by 2–10 TW laser pulses. Recent particle-in-cell (PIC) simulations have predicted that quasimonoenergetic collimated GeV electrons can be generated by focusing chirped intense lasers pulse into pure nitrogen gas and using ionization injection.<sup>19</sup> In 2013, Mo *et al.*<sup>20</sup> reported quasimonoenergetic electron beams with maximum energy  $>0.5$  GeV and 2 mrad divergence were produced in pure nitrogen gas via ionization-injection LWFA with 80 TW laser pulses. Neon and helium belong to the same group in the periodic table, but neon has higher Z. Inside neon atomic structure, there are eight outer-shell (L) electrons and two inner-shell (K) electrons moving around the nucleus. It is rather easy to remove the eight L-shell electrons by ionization using intense laser pulses (laser intensity of  $>2 \times 10^{17} \text{ W/cm}^2$  is required), however, an extremely high laser intensity of the order of  $10^{20} \text{ W/cm}^2$  is required to ionize K-shell electrons.<sup>21</sup>

As the LWFA acceleration in pure neon gas has not been experimentally explored yet, we have a near-term plan on using tightly focused 200 TW laser pulses to stimulate the ionization-induced injection in neon. In this paper, we report the initial step toward this goal where we experimentally study the LWFA of 40–100 MeV electron beams in neon at laser intensities in the range of  $10^{18} \text{ W/cm}^2$ .

The experiments were carried out at the 200 TW, 30 fs, 10 Hz Ti:Sapphire laser facility (Amplitude Technologies Co. Ltd.), located at the Key Laboratory for Laser Plasmas of Shanghai Jiao Tong University, Shanghai, China. A linearly polarized 800 nm laser pulse is focused onto a 4 mm supersonic gas jet target (A2-6443-FL, Smart Shell Co., Ltd.) with energies of 0.5–1.5 J ( $\sim 17$ –50 TW) and pulse duration of 30 fs. The 10.5-cm-diameter laser pulses were focused by

<sup>a)</sup>Electronic mail: nasr@sjtu.edu.cn

<sup>b)</sup>Electronic mail: jzhang1@sjtu.edu.cn

a 2 m focal length off-axis parabolic mirror, OAP (TYDEX Research and Industrial Optics) onto the neon gas jet target. The diameter  $d_0$  (FWHM) of the focal spot is measured to be  $32.5 \mu\text{m}$  and the Strehl ratio was 0.4–0.45. The Rayleigh range based on the  $1/e^2$  intensity radius of  $w_0 = 27.6 \mu\text{m}$  is thus  $Z_R = \pi w_0^2 / \lambda \approx 3 \text{ mm}$ , where  $\lambda$  is the laser wavelength. The focused peak laser intensity and the corresponding normalized vector potential,  $a_0$ , are around  $0.7\text{--}2.1 \times 10^{18} \text{ W/cm}^2$  and 0.6–1.0, respectively, in our experiments. Assuming the charge state of neon is  $6+$ ,<sup>21</sup> the plasma electron density ( $n_e$ ) is estimated to vary from  $1.5 \times 10^{18}$  to  $6.6 \times 10^{19} \text{ cm}^{-3}$  for backing pressures of the gas jet ranging from 0.3 to 13.2 atm. The gas jet plasma was previously characterized by the forward-Raman scattering, and by interferometry,<sup>22,23</sup> the results agrees well with the manufacturer's characterization.<sup>24</sup> To achieve the designed gas density, the gas jet solenoid has to be triggered 4.5 ms prior the arrival of the laser pulse.

An integrating current transformer (ICT-055-070-20:1, Bergoz) was used to measure the accelerated electron beam charge. A  $12.5 \mu\text{m}$  thick aluminum foil was kept between the gas jet and the ICT to block the laser light after interaction. A DRZ fluorescent screen (DRZ-PLUS, Mitsubishi Chem. Corp.), imaged into a 14-bit CCD camera (PCO. Pixelfly usb), was used for the online diagnostics of the accelerated electron beam spatial profile and pointing angle. The energy spectrum of the accelerated electrons was measured with a single shot electron spectrograph consisting of a C-shaped dipole magnet composed of two rectangle permanent magnets of  $6$  (length)  $\times$   $4$  (width)  $\text{cm}^2$ , with 1 cm pole gap, to deflect the electrons on the DRZ screen placed 17.3 cm away from the magnet end, the effective magnetic field was  $\sim B_{\text{eff}} = 0.9 \text{ T}$ . The magnetic field intensity between the pole pieces has been measured and provided into a MATLAB code which calculates the relativistic electron beam trajectory by solving the Lorentz equation of motion given the measured 2D  $B$ -field map. A top-view monitoring system, with  $0.5\times$  magnification, composed of another 14-bit CCD camera, was used to observe the laser-plasma interaction through imaging of  $2\omega$  nonlinear Thomson side scattering of the laser-plasma radiation.

Fig. 1 shows an electron beam spatial profile and the corresponding plasma channel obtained using 0.92 J of laser energy and at a neon electron density of  $5.0 \times 10^{18} \text{ cm}^{-3}$ . This electron beam has almost circular profile. The electron beam divergence angle (FWHM) was 3.2 mrad in horizontal and 3.3 mrad in vertical directions; these low divergences are, in fact, typical features for LWFA electron beams from He and H plasmas (see Ref. 25 and most of the cited references). And the length of plasma channel for generating this electron beam was around 0.8 mm for this laser shot.

Fig. 2 shows raw electron beam energy spectra obtained at the neon electron density of  $6.0 \times 10^{18} \text{ cm}^{-3}$  for a laser energy of  $\sim 1 \text{ J}$ . Fig. 2(c) presents the corresponding lineouts of the electron data, which have been deconvoluted to give the number of electrons per MeV. Note that the bright features visible at the highest energy as seen in Figs. 2(a) and 2(b) manifest themselves as peaks in Fig. 2(c); the figure shows good quasi-monoenergetic features, however it also shows a large fluctuation. A maximum peak electron energy

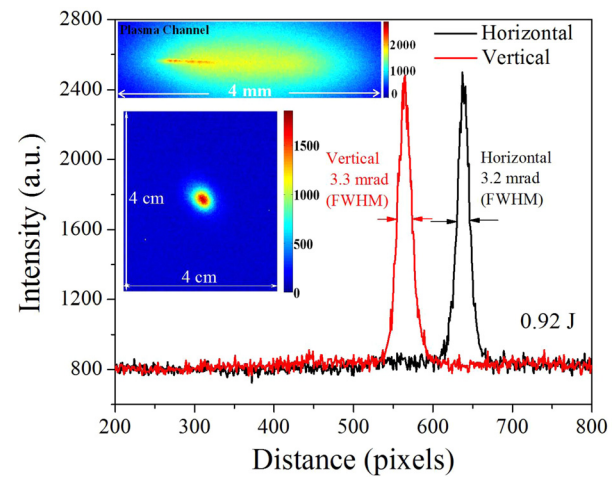


FIG. 1. Electron beam spatial profile on the DRZ captured by a synchronized 14-bit CCD; it is generated from neon at the plasma density  $n_e = 5.0 \times 10^{18} \text{ cm}^{-3}$  and 0.92 J laser energy. The inset is the corresponding laser-plasma channel.

of  $90 \pm 10 \text{ MeV}$  (Fig. 2(a)) was measured at this plasma density, with a divergence angle (FWHM) of  $2 \pm 0.2 \text{ mrad}$ . The energy spread in this case is relatively large, and the beam charge is  $\sim 41 \text{ pC}$ . However, as shown in Fig. 2(c), a monoenergetic beam at 60 MeV with  $\sim 41 \text{ pC}$  of charge is observed. The measurement statistics show that  $\sim 67\%$  of total shots observing electrons gave quasimonoenergetic electron peaks with energy greater than 80 MeV.

Figs. 3(a)–3(l) show the electron beam spatial profiles and beam charge generated at different plasma densities and

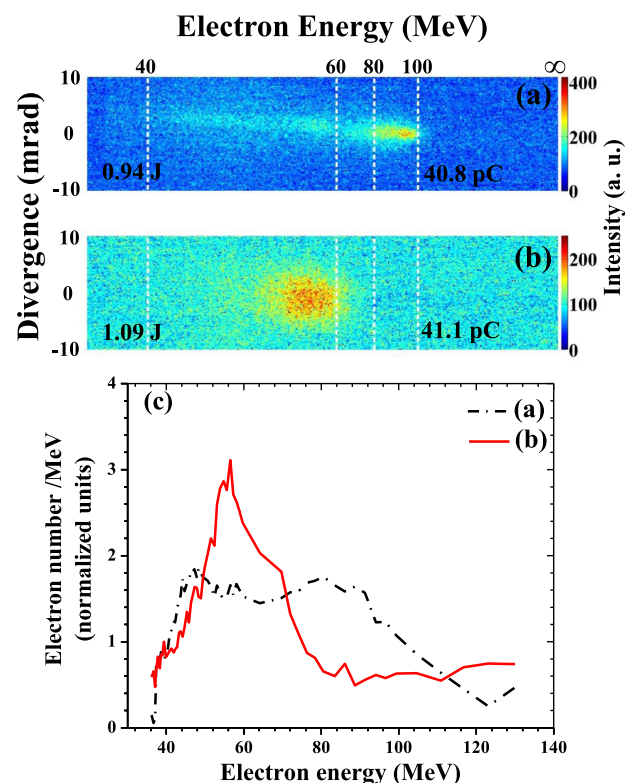


FIG. 2. (a)–(b) Raw electron energy spectra on the DRZ recorded at  $n_e = 6.0 \times 10^{18} \text{ cm}^{-3}$ . (c) The corresponding accelerated electron number density per MeV.



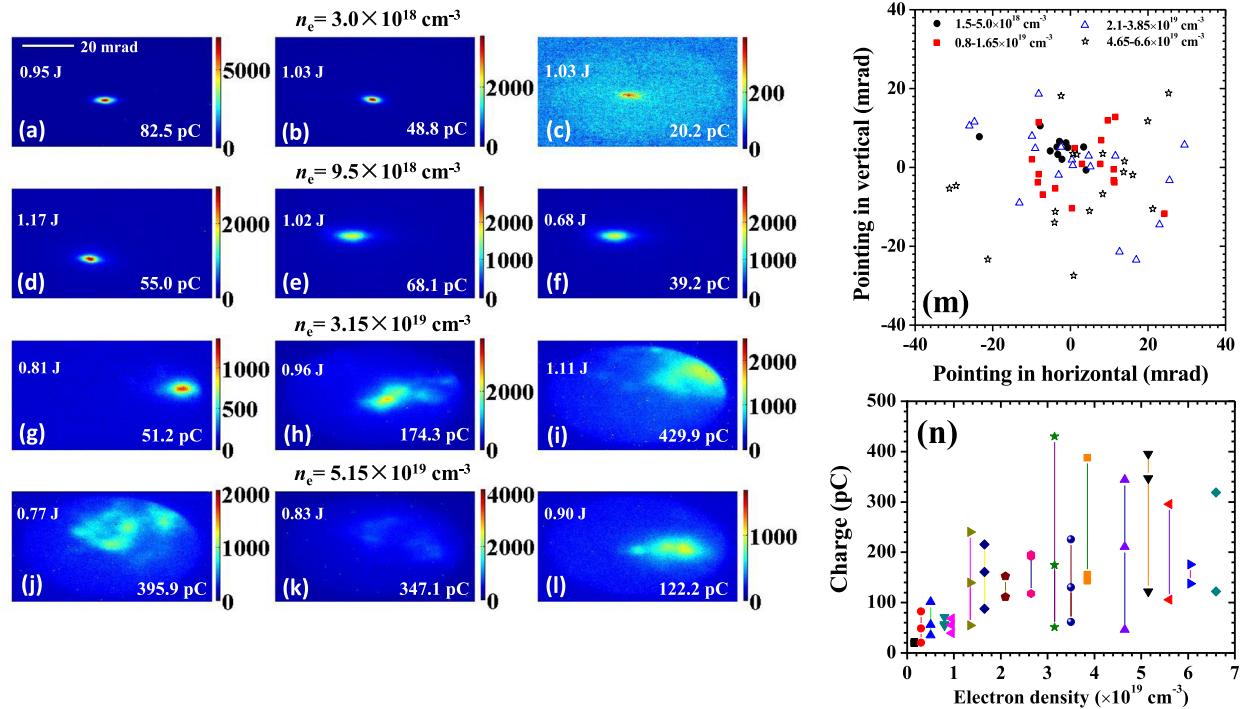


FIG. 3. Typical raw data of electron bunches generated from pure neon at different plasma densities: (a)–(c)  $n_e = 3.0 \times 10^{18} \text{ cm}^{-3}$ ; (d)–(f)  $n_e = 9.5 \times 10^{18} \text{ cm}^{-3}$ ; (g)–(i)  $n_e = 3.15 \times 10^{19} \text{ cm}^{-3}$ ; (j)–(l)  $n_e = 5.15 \times 10^{19} \text{ cm}^{-3}$ . All the data are obtained in the same color range where the brightness represents the flux of the electrons in arbitrary units. (m) Pointing angle stability graph of the electron beam at different plasma density range. (n) The measured electron beam charge versus the neon plasma densities.

laser energies. Below the density of  $3.0 \times 10^{18} \text{ cm}^{-3}$ , the divergence of the electron beam was  $\sim 4$  mrad. When the density increases up to  $5.15 \times 10^{19} \text{ cm}^{-3}$ , the electron beam divergence increases and then filaments into multiple beamlets, and the total beam divergence expands to  $\sim 41$  mrad. The pointing angle stability of the electron beam against the plasma density is shown in Fig. 3(m). Each data point corresponds to the position of a single electron beam on the DRZ screen, which translates into angles in milliradians. It is obvious that the electron beam pointing angle is minimal at low densities ( $1\text{--}5 \times 10^{18} \text{ cm}^{-3}$ ). However, by increasing the plasma density the electron beam pointing stability deteriorates significantly. Fig. 3(n) shows the electron beam charge as a function of the plasma density. It is shown that, generally the electron beam charge increases dramatically from  $\sim 10$  pC to 430 pC as the electron density increases from  $1.5 \times 10^{18} \text{ cm}^{-3}$  to  $5.15 \times 10^{19} \text{ cm}^{-3}$ . After that we see it drops to  $\sim 100$  pC level. However, we still see shot to shot fluctuations in the charge, which is believed to be due to the laser energy fluctuations. Despite the fluctuations in the charge even at the same density, the trend of for the charge enhancement with the plasma density is obvious in Fig. 3(n). It is also clear that the fluctuations increase at higher densities. It is shown that when the plasma density was lower than  $1.0 \times 10^{19} \text{ cm}^{-3}$ , which we call “stable region,” the typical electron beam had a high-quality; the divergence was a few mrad, the beam-pointing was most likely less than  $\pm 5$  mrad (in vertical direction) and the electron charge was tens pC. When the plasma density is higher than  $3.0 \times 10^{19} \text{ cm}^{-3}$ , which we call “unstable region,” low-quality electron beams which breakup into multiple beamlets

are generated. The total beam divergence expands to more than 40 mrad in two directions, the beam-pointing stability drops.

To get a possible explanation for the process of multiple electron beam generation, we have performed a few two-dimensional (2D) particle-in-cell (PIC) simulations by using the VLPL code. In the simulation, a laser pulse with normalized laser intensity of  $a = a_0 \exp(-t^2/L^2) \exp(-r^2/w^2)$ , where  $a_0 = eE/m\omega c = 0.82$ ,  $L = 30$  fs,  $w = 27.6 \mu\text{m}$  is injected into gas plasmas with density of  $8 \times 10^{18} \text{ cm}^{-3}$  (corresponding to Figs. 4(a) and 4(b) and  $4 \times 10^{19} \text{ cm}^{-3}$  (corresponding to Figs. 4(c) and 4(d)). Figures 4(a) and 4(c) show the longitudinal wakefield when two different plasma densities are used. As we can see, for a low plasma density condition the wakefield has a clean and regular profile and only exists along the laser propagation axis. However, when the density increases multiwakefield structures appear, and the wake structure shows axis symmetry. In this 2D simulations, both wakefields above and below the axis wakefield appear. The corresponding 2D electron density distributions for the two cases are shown in Figs. 4(b) and 4(d), respectively. As we can see, in the low density plasma case only electron beams on axis appears. However, at the high density case multiple electron beamlets appear in the multitransverse wakefield structures. The electrons on the side wakes seem to be injected into later wake buckets and the simulation results show that they have lower energies than the central electrons. These electrons are self-injected and strongly depend on the pulse evolution. In the 2D-slab simulations, we found although the wake shows nearly axis symmetry, such side electron injection and acceleration do not.

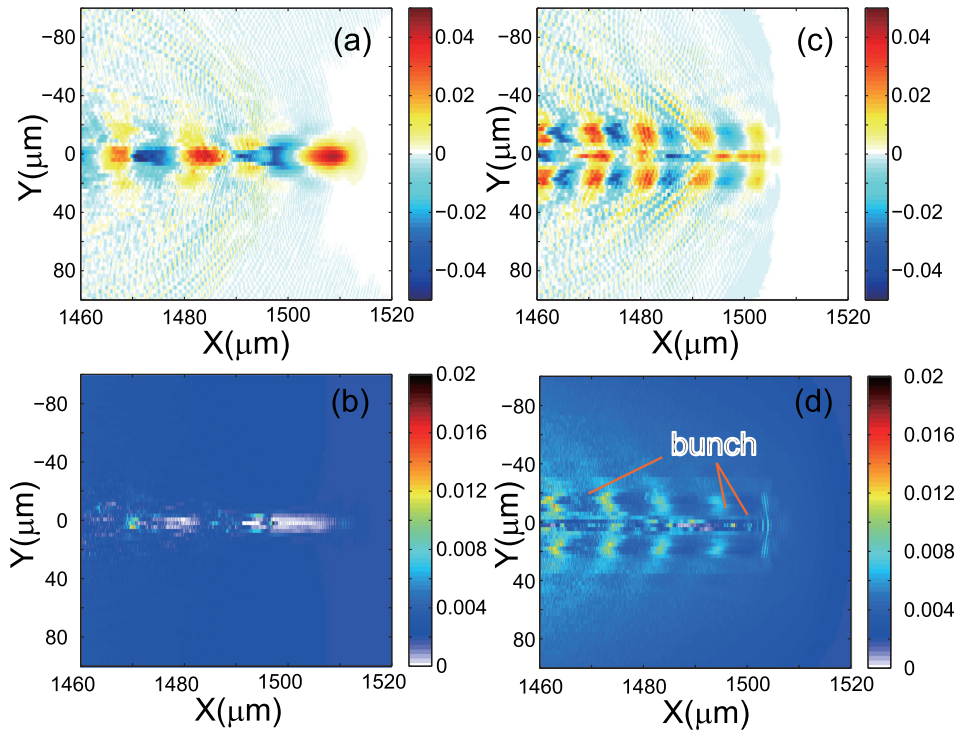


FIG. 4. Two-dimensional PIC simulation results using the VLPL code.

To summarize, the simulations are qualitatively consistent with our experimental observations (shown in Fig. 3). The reason is just because of the laser pulse evolution in the high density plasma, especially the transverse splitting of the laser pulse. In our simulation, the laser self-focusing dominates such evolution. In the high plasma density condition, the transverse laser profile evolves into multi peak structures and the pulse cannot be self-focused into a tight spot. When the pulse defocus again, multiwake appears.

According to the barrier-suppression ionization model for high-intensity laser-atom interaction, the effective appearance intensity  $I_{\text{app}}$  for ions created with charge  $Z$  can be calculated by

$$I_{\text{app}} \cong 4 \times 10^9 \left( \frac{E_{\text{ion}}}{\text{eV}} \right)^4 Z^{-2} \text{ W/cm}^2, \quad (1)$$

where  $E_{\text{ion}}$  is the ionization potential of the ion or atom with charge  $(Z-1)$ .<sup>26</sup> Thus, we can estimate the appearance intensities of neon ions which have different charge states. It should be mentioned that the collisional-ionization process which is important for long laser pulses interacting with very high plasma densities (laser-solid interaction) does not play a significant role in the present case. Here our laser pulse is extremely short and the density is far below critical density. In our experiment and at low densities (Figs. 3(a)–3(f)), we *only* observed the electron beam generation when the laser intensity was  $\geq 1.4 \times 10^{18} \text{ W/cm}^2$ , and at least  $1.0 \times 10^{18} \text{ W/cm}^2$  for the higher densities (Figs. 3(g)–3(l)). At those moderate laser intensities and according to our 2D-PIC simulation results, the electron injection mechanism is *the well-known* transverse self-injection where the L-shell electrons, which are ionized and initially displaced by the laser's ponderomotive force, are pulled back by the ions at the base of the plasma cavity (bubble) and are injected into the bubble

there.<sup>27</sup> We expect the ionization induced injection in the neon's K-shell electrons to take place at much higher laser intensities where the electrons will be injected longitudinally<sup>28</sup> through the laser pulse which will result in higher quality beams, that is to be verified experimentally in the future work.

In conclusion, we report the laser wakefield acceleration in pure neon gas and generated electron beams with a reasonable quality and stability. At a relatively high density, we observed multiple electron beamlets which has been interpreted by simulations to be the result of breakup of the laser pulse into multiple filaments in the plasma. Each filament drives its own wakefield and generates its own electron beamlet.

This work was supported by the National “973” Program of China (Grant No. 2013CBA01504), and the National Natural Science Foundation of China (Grant Nos. 11121504, 11175119, 11374209, and 11334013).

<sup>1</sup>T. Tajima and J. M. Dawson, *Phys. Rev. Lett.* **43**, 267 (1979).

<sup>2</sup>S. Kneip, S. R. Nagel, S. F. Martins, S. P. D. Mangles, C. Bellei, O. Chekhlov, R. J. Clarke, N. Delerue, E. J. Divall, G. Doucas *et al.*, *Phys. Rev. Lett.* **103**, 035002 (2009).

<sup>3</sup>N. A. M. Hafz, T. M. Jeong, I. Choi, S. K. Lee, K. H. Pae, V. V. Kulagin, J. H. Sung, T. J. Yu, K. Hong, T. Hosokai *et al.*, *Nature Photon.* **2**, 571 (2008).

<sup>4</sup>C. E. Clayton, J. E. Ralph, F. Albert, R. A. Fonseca, S. H. Glenzer, C. Joshi, W. Lu, K. A. Marsh, S. F. Martins, W. B. Mori *et al.*, *Phys. Rev. Lett.* **105**, 105003 (2010).

<sup>5</sup>W. P. Leemans, B. Nagler, A. J. Gonsalves, C. Toth, K. Nakamura, C. G. R. Geddes, E. Esarey, C. B. Schroeder, and S. M. Hooker, *Nature Phys.* **2**, 696 (2006).

<sup>6</sup>J. E. Ralph, C. E. Clayton, F. Albert, B. B. Pollock, S. F. Martins, A. E. Pak, K. A. Marsh, J. L. Shaw, A. Till, J. P. Palastro *et al.*, *Phys. Plasmas* **17**, 056709 (2010).

<sup>7</sup>D. H. Froula, C. E. Clayton, T. Doppner, K. A. Marsh, C. P. J. Barty, L. Divol, R. A. Fonseca, S. H. Glenzer, C. Joshi, W. Lu *et al.*, *Phys. Rev. Lett.* **103**, 215006 (2009).

- <sup>8</sup>S. P. D. Mangles, C. D. Murphy, Z. Najmudin, A. G. R. Thomas, J. L. Collier, A. E. Dangor, E. J. Divall, P. S. Foster, J. G. Gallacher, C. J. Hooker *et al.*, *Nature* **431**, 535 (2004).
- <sup>9</sup>A. Pak, K. A. Marsh, S. F. Martins, W. Lu, W. B. Mori, and C. Joshi, *Phys. Rev. Lett.* **104**, 025003 (2010); M. Chen, Z. M. Sheng, Y. Y. Ma, and J. Zhang, *J. Appl. Phys.* **99**, 056109 (2006); M. Chen, E. Esarey, C. B. Schroeder, C. G. R. Geddes, and W. P. Leemans, *Phys. Plasmas* **19**, 033101 (2012).
- <sup>10</sup>C. McGuffey, A. G. R. Thomas, W. Schumaker, T. Matsuoka, V. Chvykov, F. J. Dollar, G. Kalintchenko, V. Yanovsky, A. Maksimchuk, and K. Krushelnick, *Phys. Rev. Lett.* **104**, 025004 (2010).
- <sup>11</sup>M. Tao, N. A. M. Hafz, S. Li, M. Mirzaie, A. M. M. Elsieid, X. Ge, F. Liu, T. Sokollik, L. Chen, Z. Sheng, and J. Zhang, *Phys. Plasmas* **21**, 073102 (2014).
- <sup>12</sup>M. Z. Mo, A. Ali, S. Fourmaux, P. Lassonde, J. C. Kieffer, and R. Fedosejevs, *Appl. Phys. Lett.* **102**, 134102 (2013).
- <sup>13</sup>F. V. Hartemann, D. J. Gibson, W. J. Brown, A. Rouse, K. Ta Phuoc, V. Malka, J. Faure, and A. Pukhov, *Phys. Rev. ST Accel. Beams* **10**, 011301 (2007).
- <sup>14</sup>S. P. D. Mangles, G. Genoud, S. Kneip, M. Burza, K. Cassou, B. Cros, N. P. Dover, C. Kamperidis, Z. Najmudin, A. Persson *et al.*, *Appl. Phys. Lett.* **95**, 181106 (2009).
- <sup>15</sup>Z. L. Chen, C. Unick, N. Vafaei-Najafabadi, Y. Y. Tsui, R. Fedosejevs, N. Naseri, P. E. Masson-Laborde, and W. Rozmus, *Laser Part. Beams* **26**, 147 (2008).
- <sup>16</sup>M. Adachi, E. Miura, S. Kato, K. Koyama, S. Masuda, T. Watanabe, A. Ogata, H. Okamoto, and M. Tanimoto, *Laser Phys. Lett.* **3**, 79 (2006).
- <sup>17</sup>H. Kotaki, Y. Hayashi, K. Kawase, M. Mori, M. Kando, T. Homma, J. K. Koga, H. Daido, and S. V. Bulanov, *Plasma Phys. Controlled Fusion* **53**, 014009 (2011).
- <sup>18</sup>N. Hafz, G. H. Kim, C. Kim, and H. Suk, *Int. J. Mod. Phys. B* **21**, 398 (2007).
- <sup>19</sup>K. P. Singh and V. Sajal, *Phys. Plasmas* **16**, 043113 (2009).
- <sup>20</sup>M. Z. Mo, A. Ali, S. Fourmaux, P. Lassonde, J. C. Kieffer, and R. Fedosejevs, *Appl. Phys. Lett.* **100**, 074101 (2012).
- <sup>21</sup>R. Fedosejevs, X. F. Wang, and G. D. Tsakiris, *Phys. Rev. E* **56**, 4615 (1997).
- <sup>22</sup>N. M. Hafz, I. W. Choi, J. H. Sung, H. T. Kim, K.-H. Hong, T. M. Jeong, and T. J. Yu, *Appl. Phys. Lett.* **90**, 151501 (2007).
- <sup>23</sup>W. Yan, L. Chen, D. Li, L. Zhang, N. A. M. Hafz, J. Dunn, Y. Ma, K. Huang, Luning Su, M. Chen *et al.*, *Proc. Natl. Acad. Sci. USA* **111**, 5825 (2014).
- <sup>24</sup>T. Hosokai, K. Kinoshita, T. Watanabe, K. Yoshii, T. Ueda, A. Zhidokov, M. Uesaka, K. Nakajima, M. Kando, and H. Kotaki, in *8th European Particle Accelerator Conference (EPAC), Paris, France, 3–7 June 2002* (2002), pp. 981.
- <sup>25</sup>S. Li, N. A. M. Hafz, M. Mirzaie, X. Ge, T. Sokollik, M. Chen, Z. Sheng, and J. Zhang, *J. Appl. Phys.* **116**, 043109 (2014).
- <sup>26</sup>P. Gibbon, *Short Pulse Laser Interactions With Matter* (Imperial College Press, London, UK) pp. 20–23.
- <sup>27</sup>A. Pukhov and J. Meyer-ter-Vehn, *Appl. Phys. B* **74**, 355 (2002).
- <sup>28</sup>S. Corde, C. Thaury, A. Lifschitz, G. Lambert, K. Ta Phuoc, X. Davoine, R. Lehe, D. Douillet, A. Rouse, and V. Malka, *Nat. Commun.* **4**, 1501 (2013).